JMEPEG (2009) 18:1209–1217
DOI: 10.1007/s11665-009-9359-0

1059-9495/$19.00

# A Model to Predict Recrystallization Kinetics in Hot Strip Rolling Using Combined Artificial Neural Network and Finite Elements

*M. Seyed Salehi and S. Serajzadeh*

*(Submitted February 1, 2008; in revised form November 25, 2008)*

**A thermo-mechanical model has been developed to establish a coupled heat conduction and plastic flow analysis in hot-rolling process. This model is capable of predicting temperature, strain, and strain rate distributions during hot rolling as well as the subsequent static recrystallization fraction and grain size changes after hot deformation. Finite element and neural network models are coupled to assess recrystallization kinetics after hot rolling. A new algorithm has been suggested to create differential data sets to train the neural network. The model is then used to predict histories of various deformation variables and recrystallization kinetics in hot rolling of AA5083. Comparison between the theoretical and the experimental data shows the validity of the model.**

**Keywords** aluminum AA5083, artificial neural network, finite element analysis, hot rolling, static recrystallization

## 1. Introduction

In rolling process, geometric accuracy and mechanical properties can be determined by rolling parameters, such as reduction, rolling temperature, rolling speed, and interstand cooling rate. Thus, thermal, mechanical, and microstructural models should be coupled to accurately understand materials behavior during and after hot rolling. Presently, the combination of physical metallurgy with numerical techniques makes it possible to predict microstructural evolution of the hot-rolled product (Ref 1-3). The finite element method which has been employed for simulation of hot rolling of plates is a powerful tool in the modeling of deformation processes and it has been applied widely to model the hot strip rolling by many authors (Ref 1-3). In addition, a combination of the finite element analysis and metallurgical models has been proposed to predict grain size distributions and recrystallization kinetics in hot strip rolling operations (Ref 4). Many researchers have also used Avrami's equation to assess the grain size and recrystallization kinetics during and after hot rolling. Note that Avrami's equation should be used under isothermal conditions, however, for nonisothermal problems such as rolling process researchers have employed the additivity rule together with Avrami's equation (Ref 5-7). In fact, the additivity rule is considered as a special algorithm for predicting the nonisothermal transformation on the basis of known isothermal kinetic equation.

**M. Seyed Salehi** and **S. Serajzadeh**, Department of Materials Science and Engineering, Sharif University of Technology, Azadi Ave., P.O. Box 11365-9466, Tehran, Iran. Contact e-mail: serajzadeh@sharif.edu.

However, determination of grain distribution is the main problem in such models. For these situations, numerical calculation and artificial intelligence can be used efficiently. Recently, artificial neural networks, ANN, were used for various metallurgical problems such as simulation of TTT and CCT diagrams (Ref 8, 9) and prediction of mechanical properties (Ref 10).

In the present study, a two-dimensional thermo-mechanical model is developed to predict temperature, strain rate, and strain distributions during hot rolling as well as to assess the kinetics of static recrystallization after rolling. To do so, a finite element analysis is coupled with a neural network model. At the first stage, temperature, strain, and strain fields within the hot-rolled metal are predicted by means of a two-dimensional finite element analysis and then, the kinetics of static recrystallization and grain size variations are modeled by combining a thermal analysis based on the finite elements with a neural network model. In the final stage, the proposed model is examined for hot rolling of AA5083.

## 2. Thermo-Mechanical Model

In hot strip rolling process, the ratio of strip width to its thickness is large, then plane strain model may be used where the strain and the temperature gradients in width direction may be ignored. Thus in this work, a two-dimensional finite element analysis is employed to predict temperature, strain, and strain rate in the rolling of slabs as well as the temperature distribution within the work-rolls. In addition, because of symmetry within the deformation zone, only half of plate is taken into account. In the model, the interaction of the thermal and mechanical phenomena is considered. The flow stress is coupled to the rolling temperature, strain rate, and strain. At the same time, the friction and the heat of deformation cause an increase in the temperature of the metal and the work-roll surface. Hence, thermal and mechanical

models should be coupled to include the effects of the abovementioned factor simultaneously.

For a rigid viscoplastic material, the variational principle of potential energy is expressed as below (Ref 11) where the real velocity field minimizes the following functional.

$$\pi = \iiint_{v} \bar{\sigma}\,\dot{\bar{\varepsilon}} dv + \iint_{s_f} \tau_f \Delta V_f ds + \frac{K}{2} \iiint_{v} \dot{\varepsilon}_v^2 dv \qquad \text{(Eq 1)}$$

Here $\bar{\sigma}$ is the equivalent stress, $\dot{\bar{\varepsilon}}$ the equivalent strain rate, $\Delta V_f$ the velocity discontinuity across the frictional surface, $\tau_f$ the frictional shear stress, $K$ is a large positive constant, and $\dot{\varepsilon}_v$ volumetric stain rate. Due to existing symmetry, the velocity in the $y$-direction is zero at the center line. On the contact surface of the work-roll and the slab, the velocity in normal direction of contact surface should be set to zero.

On the contact surface, frictional stress between the work-roll and the metal must be considered; the following velocity-dependent equation has been employed to include the change in relative velocity (Ref 11).

$$\tau_f = -m_k \tau_s \left( \frac{2}{\pi} \tan^{-1} \left( \frac{\Delta V_f}{V_a} \right) \right) \qquad \text{(Eq 2)}$$

where $\tau_s$ is the shear flow stress, $m_k$ friction factor, and $V_a$ a small positive constant. The temperature distribution in the slab and the work-roll may be determined by Fourier's law of two-dimensional heat conduction as below:

$$\frac{\partial}{\partial x}\left( k \frac{\partial T}{\partial x} \right) + \frac{\partial}{\partial y}\left( k \frac{\partial T}{\partial y} \right) + \dot{q} = \rho c \frac{\partial T}{\partial t} \qquad \text{(Eq 3)}$$

where $k$ is the coefficient of heat conduction, $\rho$ density, $c$ specific heat, and $\dot{q}$ input energy rate due to plastic deformation. During hot rolling, the rate of heat of deformation should be considered in the governing heat conduction equation, which may be calculated as follows:

$$\dot{q} = \eta \bar{\sigma} \dot{\bar{\varepsilon}} \qquad \text{(Eq 4)}$$

where $\eta$ is the efficiency of conversion coefficient. This factor usually varies between 0.9 and 0.95 in practical working conditions (Ref 11); accordingly in the present work, it has been assumed to be 0.95. To solve the abovementioned equation, it is necessary to distinguish the governing boundary and initial conditions. In contact surface of the work-roll and the slab, heat is generated owing to friction and also, thermal energy is transferred from metal to the work-rolls. Therefore, the boundary conditions on the contact zone can be expressed as:

$$k \left( \frac{\partial T}{\partial n} \right)_{\Gamma} + h_R (T - T_R) + \eta_f \tau_f \Delta V_f = 0 \qquad \text{(Eq 5)}$$

where "$n$" denotes the normal vector surface $\Gamma$, $h_R$ the heat transfer coefficient between the work-roll and the slab, and $\eta_f$ is the distribution coefficient of heat. This parameter has been assumed to be as 0.5 (Ref 12). On free surfaces, the slab is cooled by convection and radiation and thus, the following boundary conditions may be utilized:

$$k \left( \frac{\partial T}{\partial n} \right) + \lambda s (T^4 - T_\infty^4) + h_{air} (T - T_\infty) = 0 \qquad \text{(Eq 6)}$$

In the above equation, $\lambda$ is the emissivity, "$s$" Stephan's constant, $h_{air}$ convection coefficient, and $T_\infty$ the environmental temperature. It is worth noting that the finite element method and Galerkin technique (Ref 12) together with isoparametric quadrilateral elements have been used to solve the heat conduction equation and plastic deformation formulation. A code in MATLAB has been provided based on the abovementioned mathematical model using an updated Lagrangian scheme that provides a transient analysis. Direct iteration is also performed to handle the nonlinearity due to boundary conditions and material properties. The calculation flow chart is shown in Fig. 1. This flow chart includes the rolling thermo-mechanical model in conjunction with microstructural model.

## 3. Recrystallization and Neural Network Model

After the hot rolling, the microstructure is controlled by the recrystallization kinetics. In general, the recrystallization volume fraction may be expressed as follows:

$$f = X(t, T, \bar{\varepsilon}, \dot{\bar{\varepsilon}}, d) \qquad \text{(Eq 7)}$$

where "$f$" is recrystallization fraction, $\dot{\bar{\varepsilon}}$ is mean equivalent strain rate, and "$d$" is initial grain size. We assume that at the current time, $t$, temperature is $T_m^t$, equivalent strain $\bar{\varepsilon}_m^t$, mean equivalent strain rate $\dot{\bar{\varepsilon}}_m^t$, initial grain size $d_m^t$ and recrystallized fraction $f_m^t$ where "$m$" denotes node number. Taylor series expansion has been used for calculating the recrystallized volume fraction $(f_m^{t+\Delta t})$ of $m$th node at the time $t + \Delta t$ as follows.

$$f_m^{t+\Delta t} = f_m^t + \left( \frac{dX}{dt} \right)_m^t \Delta t + \left( \frac{d^2X}{dt^2} \right)_m^t \frac{\Delta t^2}{2} + O(\Delta t^3) \qquad \text{(Eq 8)}$$
$$f_m^t = 0 \quad \text{when } \dot{\bar{\varepsilon}}_m^t \neq 0$$

where $\Delta t$ is the employed time step and $O(\Delta t^3)$ is the residual part and may be ignored if the time step is selected to be small enough. Under these circumstances, the volume fraction may be described as follows:

$$f_m^{t+\Delta t} \approx f_m^t + \left( \frac{dX}{dt} \right)_m^t \Delta t + \left( \frac{d^2X}{dt^2} \right)_m^t \frac{\Delta t^2}{2} \qquad \text{(Eq 9)}$$

$$\left( \frac{dX}{dt} \right)_m^t = \varphi_m^t \left( T_m^t, \bar{\varepsilon}_m^t, \dot{\bar{\varepsilon}}_m^t, d_m^t, f_m^t \right)$$

$$\left( \frac{d^2X}{dt^2} \right)_m^t = \psi_m^t \left( T_m^t, \bar{\varepsilon}_m^t, \dot{\bar{\varepsilon}}_m^t, d_m^t, f_m^t \right)$$

$$f_m^{t+\Delta t} \approx f_m^t + \varphi_m^t \Delta t + \frac{\psi_m^t \Delta t^2}{2}$$

In hot-rolling process, the strain, strain rate, and temperature distributions within aluminum slab were investigated by the thermo-mechanical model explained in the previous section. These parameters are the factors that affect the recrystallization kinetics. These parameters were applied to train neural network and the model returns recrystallized fraction and grain size distribution. The computational procedure is given in Fig. 1.

Artificial neural networks are highly distributed interconnections of adaptive nonlinear processing elements that are capable of learning information presented to them. The connection strengths, also called the network weights, can be adapted somehow that the network's output matches a desired response. Inputs are weighted, combined, and then processed through a transfer function which controls intensity of output

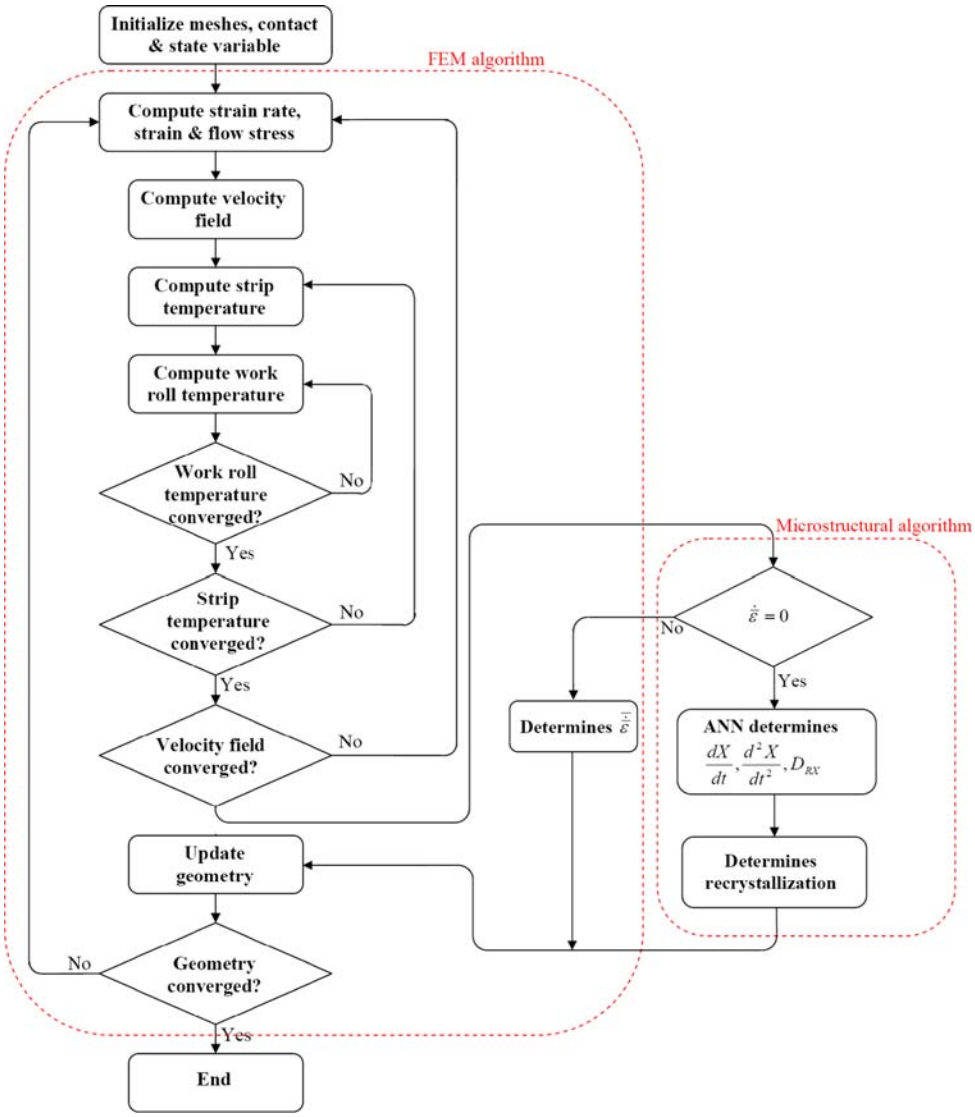


**Fig. 1** The procedure used in the thermo-mechanical and the microstructural calculations

signal. Neural networks may be used for many transfer functions, such as sigmoid, Gaussian, hyperbolic tangent, and hyperbolic secant (Ref 13). In hot-rolling process, the strain, strain rate, and temperature distribution within aluminum slab were investigated by the thermo-mechanical model explained in the previous section.

In this model, the input parameters that applied to the neural network are temperature, strain, strain rate, initial grain size, and previous recrystallized fraction. The model returns three output, i.e., $\varphi_m^t$, $\psi_m^t$ and recrystallized grain size as shown in Fig. 2.

In neural networks, two data sets are needed: one for training the network and the second one for testing the model. Data sets are created based on experimental data published in (Ref 14). The empirical data explain the relationship between recrystallized volume fraction versus time at constant temperature, strain, strain rate, and initial grain size. In the mathematical algorithm, the empirical data, recrystallized fraction versus time and time versus recrystallized fraction, have been fitted by two functions as $g(t)$ and $h(f)$. Several functions have been examined and the best fitting functions have been selected on the basis of the quality of the fit. The following exponential and logarithmic functions have been used for this purpose.

$$g_{T,\bar{\varepsilon},\dot{\bar{\varepsilon}},D0}(t) = \exp(a_1 t^{n_1}) - \exp(a_2 t^{n_2}) \quad \text{(Eq 10)}$$

$$h_{T,\bar{\varepsilon},\dot{\bar{\varepsilon}},D0}(f) = b(\ln(cf))^m \quad \text{(Eq 11)}$$

where $a_1$, $a_2$, $n_1$, $n_2$, $b$, $c$, and $m$ are determined by fitting algorithm. For doing so, curve fitting toolbox on the MATLAB is used. For calculating $\varphi$ and $\psi$, the first and the second derivatives should be determined as below:

$$\varphi|_{T,\bar{\varepsilon},\dot{\bar{\varepsilon}},d} = g'_{T,\bar{\varepsilon},\dot{\bar{\varepsilon}},d}(t) = g'_{T,\bar{\varepsilon},\dot{\bar{\varepsilon}},d} o h_{T,\bar{\varepsilon},\dot{\bar{\varepsilon}},d}(f) \quad \text{(Eq 12)}$$

$$\psi|_{T,\bar{\varepsilon},\dot{\bar{\varepsilon}},d} = g''_{T,\bar{\varepsilon},\dot{\bar{\varepsilon}},d}(t) = g''_{T,\bar{\varepsilon},\dot{\bar{\varepsilon}},d} o h_{T,\bar{\varepsilon},\dot{\bar{\varepsilon}},d}(f) \quad \text{(Eq 13)}$$

Then, data sets for training and testing of neural network can be computed with the above formulations. Figure 3 shows the flow chart of providing training and testing data sets.

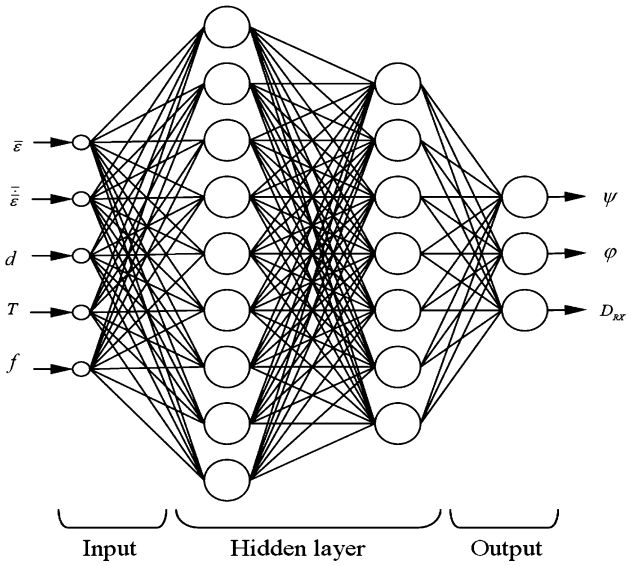


**Fig. 2** Schematic illustration of artificial neural network architecture used in this work

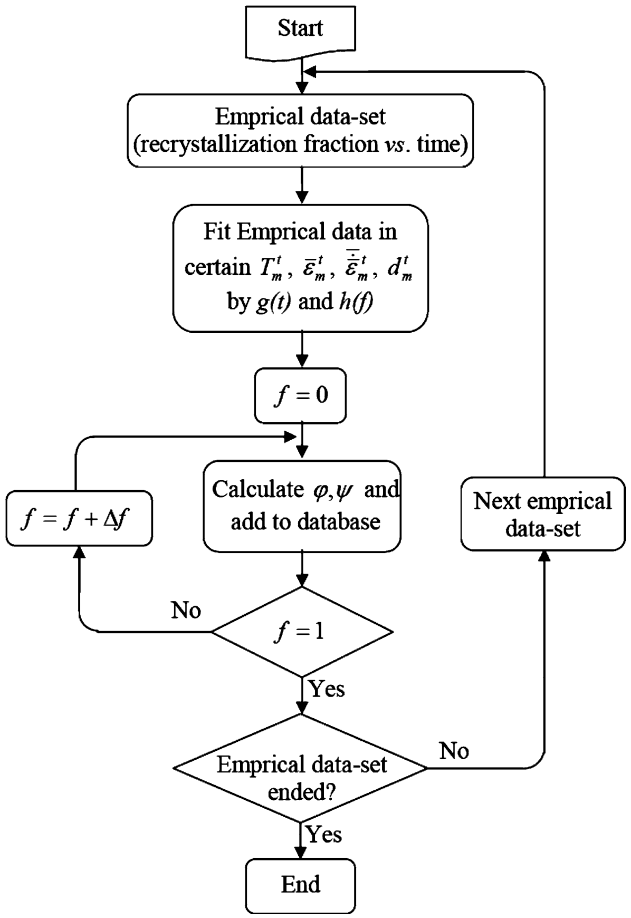


**Fig. 3** Flow chart employed for creating training and testing data sets

Neural network architecture is a very vital variable that can specify the network efficiency. Then several networks with various architectures should be examined to select optimized network. In this study, ANN architecture is a multi-layer, feed forward, and back propagation architecture. The activation function is chosen as the sigmoid function and the Bayesian regularization algorithms (BR) have been applied for training the network.

**Table 1 Chemical composition of AA5083 aluminum alloy, wt.%**

| Si | Fe | Cu | Mn | Mg | Cr | Al |
|---|---|---|---|---|---|---|
| 0.05 | 0.07 | 0.02 | 0.65 | 4.48 | 0.11 | Balance |

**Table 2 Heat conduction coefficient and specific heat of AA5083 (Ref 15)**

| Temperature, °C | Specific heat, J kg$^{-1}$ K$^{-1}$ | Coefficient conduction, W m$^{-1}$ K$^{-1}$ |
|---|---|---|
| 14 | 930 | 143.4 |
| 280 | 990 | 167.1 |
| 306 | 1010 | 170.2 |
| 410 | 1050 | 174.1 |
| 505 | 1160 | 185.4 |

## 4. Materials and Experiments

An aluminum alloy, AA5083, with the chemical composition listed in Table 1 is studied in this work. To calculate the temperature field in slab, the heat conduction coefficient and specific heat at various temperatures are shown in Table 2 (Ref 15) and the density is assumed to be 2660 kg m$^{-3}$ (Ref 15). The coefficient of heat conduction for the work-roll is taken as 32 W m$^{-1}$ K$^{-1}$, specific heat 670 J kg$^{-1}$ K$^{-1}$, and density 7800 kg m$^{-3}$. The work-roll diameter is 150 mm. The heat transfer coefficient between the work-roll and the slab is determined using the empirical equation derived in Ref 16. The strip is assumed to behave as a rigid viscoplastic material while the material behavior is described by following constitutive equation:

$$\dot{\varepsilon} = A \exp\left(\frac{-Q_{\text{def}}}{RT}\right)(\sinh(\alpha\bar{\sigma}))^m \qquad \text{(Eq 14)}$$

where "$A$," $\alpha$, and "$m$" are material constants. For this alloy, the following flow stress parameters have been utilized in the constitutive equation, $A = 2.87 \times 10^8$, $a = 0.04$ MPa$^{-1}$, $m = 2.26$, and $Q_{\text{def}} = 162500$ J mol$^{-1}$ (Ref 17, 18).

An experimental program was designed to record temperature history and recrystallized fraction and grain size of the slab in hot-rolling process. A series of single-pass rolling experiments were performed using the rolling parameters summarized in Table 3 and an initial sample thickness of 8 mm. Specimens were annealed at 450 °C for 1 h and then air cooled. A 1.5-mm diameter hole was drilled on one side of the test specimens and a K-type thermocouple was embedded in the drilled hole to record temperature history. The thermocouple logged the temperature history during hot-rolling process. Specimens were hot rolled and then quenched after given times. In the next step, specimens were prepared for optical

microscopy by mechanical polishing in the standard manner followed by chemical etching using Graf's Reagent containing 15.5 mL $HNO_3$, 0.5 mL HF, 0.3 g $Cr_2O_3$, and 84 mL water.

## 5. Result and Discussion

Based on thermo-mechanical equations and the utilized mathematical model, strain, strain rate, and temperature distributions have been predicted during and after hot rolling. Figure 4 shows the predicted and the measured temperature variations at different points of the sample #10. A peak in temperature profile can be observed in the central region which is due to the heat of deformation. However, at the surface, temperature drops abruptly due to the heat transfer between the work-roll and the slab. After hot rolling, heat conduction between surface and center decreases the temperature gradient. Figure 5 shows temperature variations in central region of the samples 1, 4, 7, and 10. Clearly, changes in rolling parameter such as reduction, rolling temperature and rolling speed cause a change in temperature profile. Figure 5 presents a comparison between measured values and those predicted by the present model. In this figure, maximum and minimum drop in temperature are observed in samples 1 and 4, respectively.

Figure 6 shows the strain rate development through thickness in specimen 10. A peak is seen in surface strain rate that occurs at the beginning of deformation. This is attributed to the sudden change of velocity boundary conditions along the

**Table 3 Rolling conditions used in the experiments**

| Specimen no. | Reduction, % | Initial temperature, °C | Rolling speed, RPM | Time prior to quench, s |
|---|---|---|---|---|
| 1 | 15 | 300 | 42 | 15 |
| 2 | 15 | 300 | 42 | 25 |
| 3 | 15 | 300 | 42 | 34 |
| 4 | 15 | 400 | 42 | 11 |
| 5 | 15 | 400 | 42 | 17 |
| 6 | 15 | 400 | 42 | 39 |
| 7 | 15 | 400 | 60 | 16 |
| 8 | 15 | 400 | 60 | 20 |
| 9 | 15 | 400 | 60 | 30 |
| 10 | 30 | 400 | 60 | 9 |

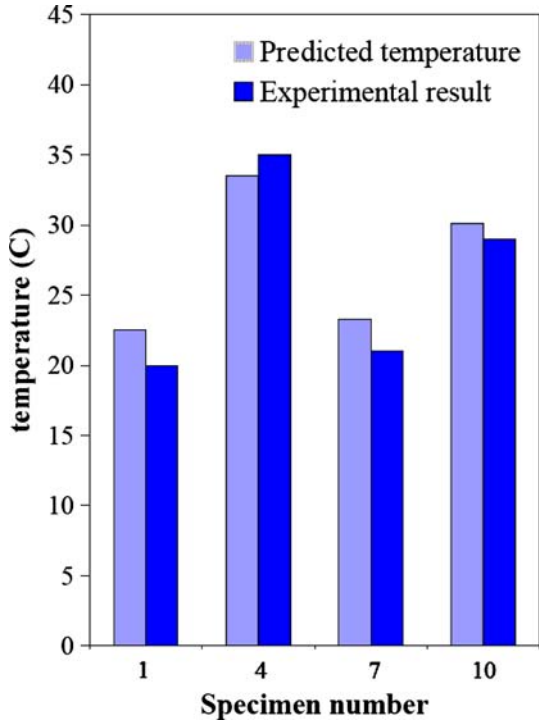


**Fig. 5** Temperature drop in central region of specimens 1, 4, 7, and 10

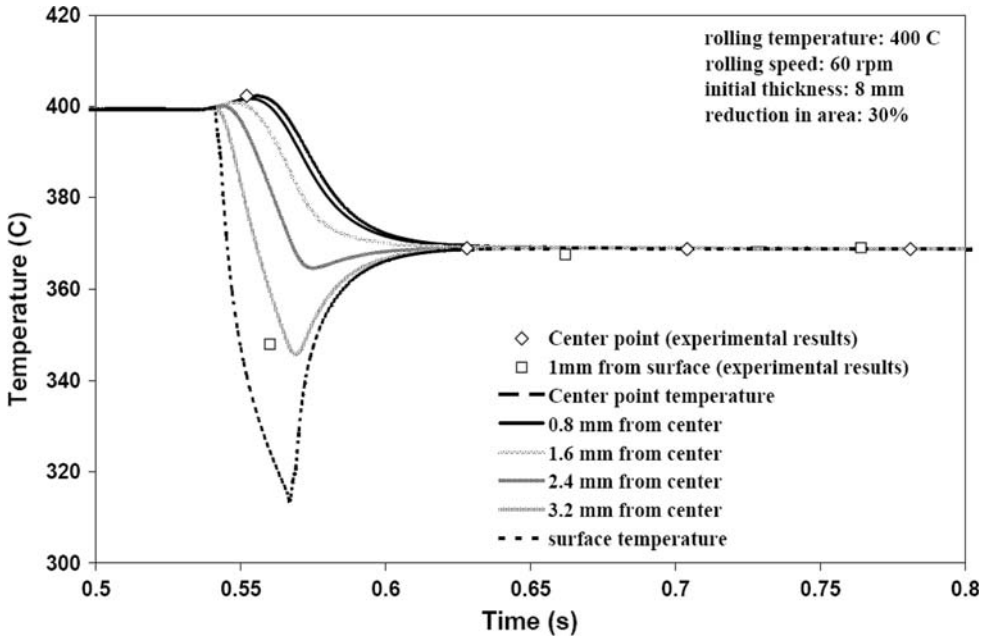


**Fig. 4** Comparison between predicted and measured temperatures for specimen 10

vertical direction. It is worth noting that the highest strain rate occurs close to the entry of the roll gap, and subsequently decreasing gradually along the contact arc as shown in Fig. 6. The amount of plastic deformation is an effective parameter in recrystallization kinetics. This parameter is also calculated in each point in deformation domain by means of the thermo-mechanical model. Figure 7 shows effective strain distribution

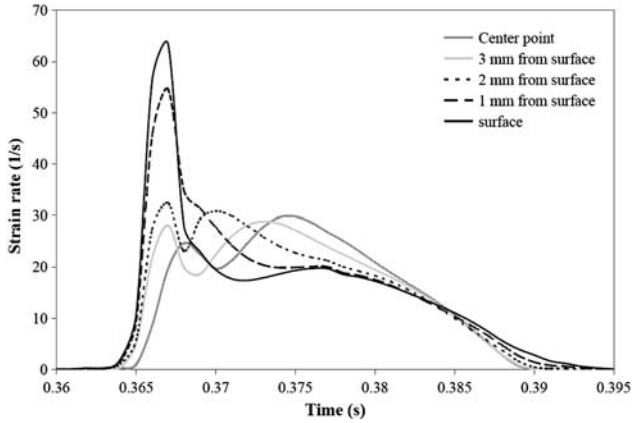


**Fig. 6** Strain rate variations along rolling direction in specimen 10

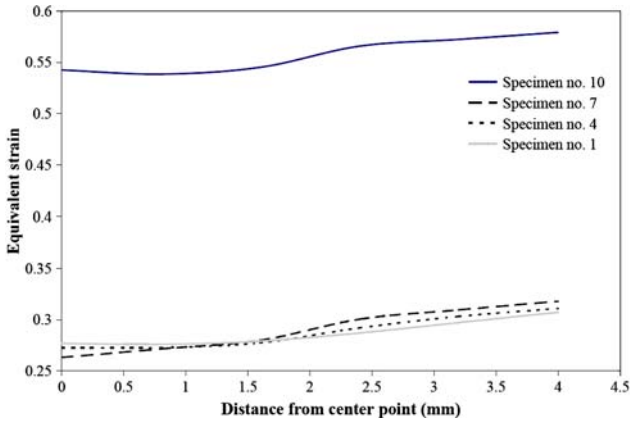


**Fig. 7** Strain distribution along thickness at the exit point of deformation zone

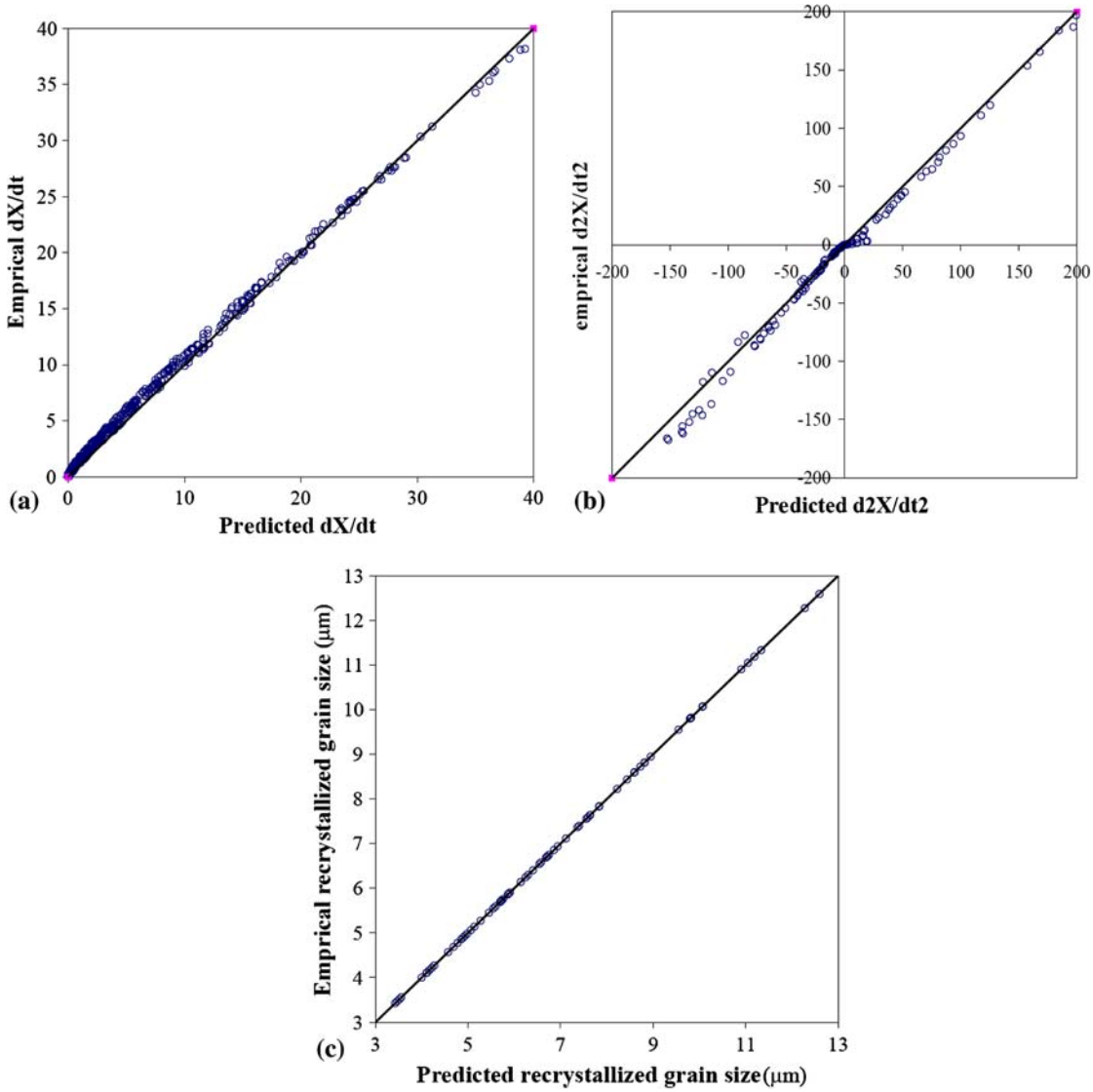


**Fig. 8** Comparison between predicted and empirical (a) $dX/dt$, (b) $d^2X/dt^2$, and (c) recrystallized grain size

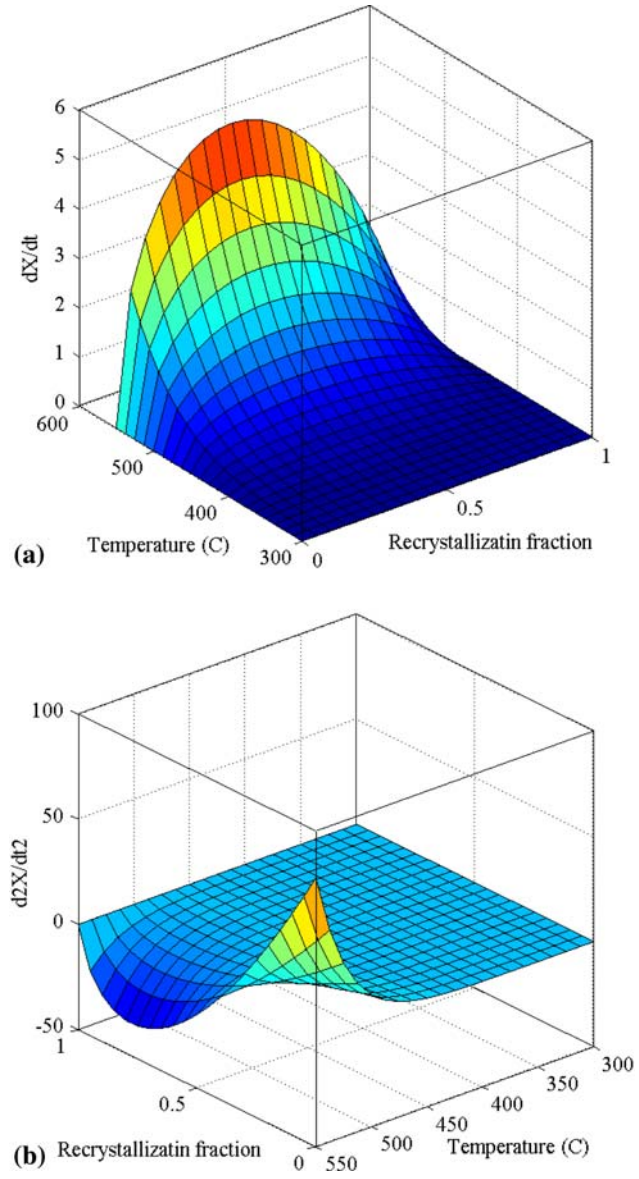


**Fig. 9** Using ANN to predict (a) $dX/dt$ and (b) $d^2X/dt^2$ in various temperatures and recrystallization fractions

along thickness direction in specimens 1, 4, 7, and 10. It can be seen that when the rolling temperature rises from 300 to 400 °C, the distribution of effective strain is also altered as shown in Fig. 7 and the flow concentration in surface zone occurs due to the effect of temperature on flow behavior. An increase in rolling speed also causes the same changes in strain distribution which is shown in Fig. 7 for specimens 4 and 7.

Proper training of the neural network requires sufficiently large training data sets. First of all, the empirical data must be fitted with fitting function. In fitting session, exponential and logarithmic functions have been utilized and at each temperature, strain, strain rate and initial grain size, and singular functions are prepared. In the following stage, the neural network has been constructed to simulate metallurgical events. In the present work, the network architecture with three hidden layers is found to be the best suited model. The ANN architecture used in the part is a 5:11:9:9:3 layer architecture. These values are found to be optimum values by trial and error.

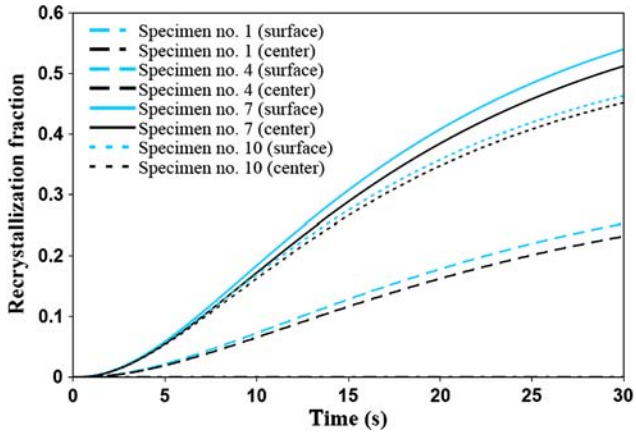


**Fig. 10** Predicted recrystallized fraction in specimens 4, 7, and 10

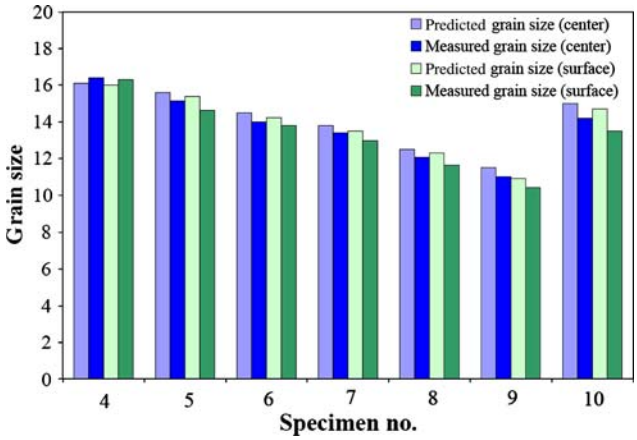


**Fig. 11** Comparison between measured and predicted grain size in center and surface of hot-rolled samples

$d/100$, $d$ is initial grain size, $T/1000$, $f$, $\bar{\varepsilon}$ and $\dot{\bar{\varepsilon}}$ are the input parameters and $\varphi_m^t$, $\psi_m^t$, and $D$ (recrystallized grain size) are the output parameters. The employed performance is demonstrated in Fig. 8 which shows the analysis of the network response. In this figure, a comparison between the predicted results and testing data set is illustrated. This figure shows a good performance of the neural network and therefore the employed network can be utilized for further simulation.

Figure 9 displays the predicted outputs, φ and ψ. This figure clearly delineates the anticipated drift in output values with alteration in the temperature and fraction of recrystallization. After the training is completed, the network is used to predict the amount of recrystallization fraction and grain size after hot rolling by coupling the thermo-mechanical results with the developed neural network model.

Figure 10 shows the recrystallized fraction versus time for specimens 1, 4, 7, and 10. It can be concluded that with increasing reduction per pass, recrystallization kinetics becomes slower. Indeed an increase in reduction induces a higher amount of strain, strain rate, and drop in temperature in the slab. In aluminum AA5083, temperature variation is more effective than strain and strain rate in altering recrystallization

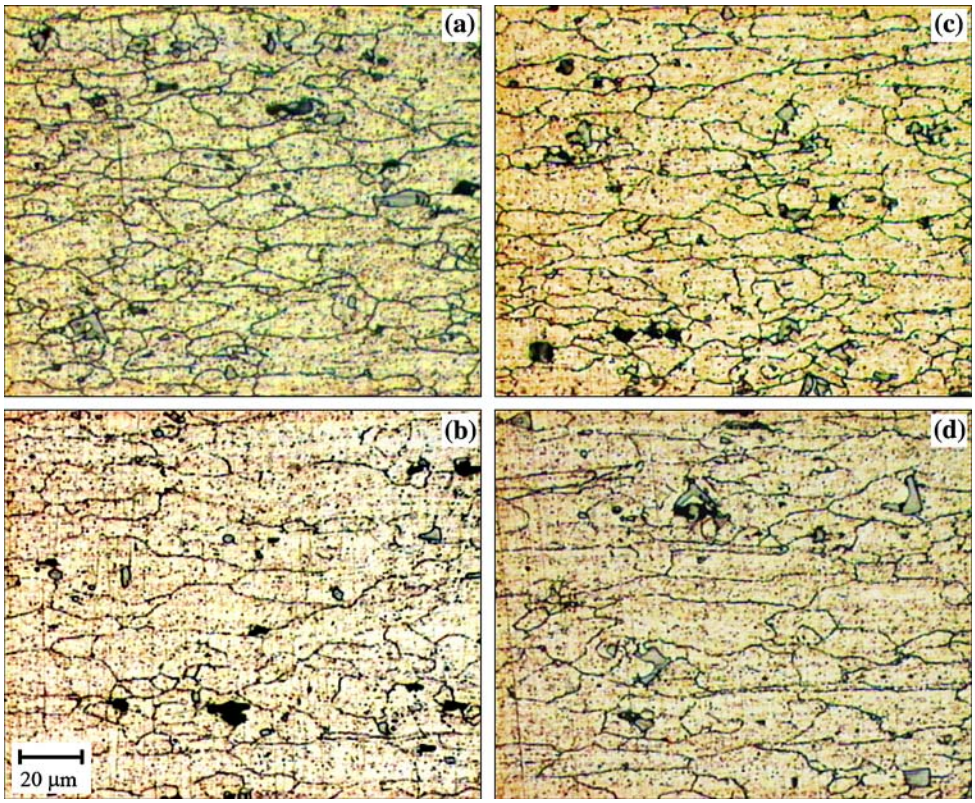


**Fig. 12** Optical micrograph, (a) sample 10 surface, (b) sample 10 center, (c) sample 7 surface, and (d) sample 7 center

kinetics. According to Fig. 10, it is observed that recrystallization kinetics increases with increasing temperature.

Recrystallization kinetics of specimen no. 1 is very slow due to low temperature of the hot-rolled metal. The influence of rolling speed on the recrystallization kinetics shows a similar tendency as displayed in Fig. 10 (specimens 4 and 7). On the other hand, increasing the rolling speed has a significant effect on the recrystallization kinetics due to an increase in the equivalent strain rate and effective strain during hot deformation.

In all specimens, recrystallization kinetics in the central region is slower than at surface region. The predicted temperature history illustrates that a severe temperature drop has occurred at the surface compared with that in the central regions due to heat losses to environment and to the work-rolls as displayed in Fig. 4. However, aluminum alloys have very good heat conductivity and therefore, the surface and center temperatures become approximately uniform after hot rolling within a relatively short time.

According to Fig. 6 and 7, strain rate and strain in slab surface are larger than those in the center points. Greater strain and strain rate in surface at uniform temperature lead to higher rate of recrystallization at the surface region. Figure 11 shows the variation of grain size at the surface and the depth of the rolled metal during single deformation pass and Fig. 12 displays grain size at the depth of the samples 7 and 10. As it is seen, there is a good agreement between the predictions and the experimental data. Regarding these figures, the grain size distribution is also inhomogeneous, resulting from the inhomogeneity in temperature, strain rate, and strain distributions. Note that in all specimens, grain size at the surface region is smaller than the grain size in the inner regions, and the predictions show the same behavior.

## 6. Conclusion

A mathematical model based on the finite element method and ANNs have been developed to predict the thermo-mechanical history and microstructural changes during hot rolling of AA5083. The model is capable of considering the effects of various process parameters, such as rolling speed, rolling temperature, and slab geometry. By comparing the model predictions with the experimental results, the performance of the model is proved for single stand hot rolling. It shows that the neural network model in conjunction with the finite element analysis established in this work can be employed to study process parameters as well as to optimize hot-rolling schedules.

### References

1. M. Toloui and S. Serajzadeh, Modelling Recrystallization Kinetics During Hot Rolling of AA5083, *J. Mater. Process. Technol.*, 2007, **184**, p 345–353
2. X. Li, M. Wang, and F. Dua, A Coupling Thermal Mechanical and Microstructural FE Model for Hot Strip Continuous Rolling Process and Verification, *Mater. Sci. Eng. A*, 2005, **408**, p 33–41
3. S. Serajzadeh, A Model for Prediction of Flow Behavior and Temperature Distribution During Warm Rolling of a Low Carbon Steel, *Mater. Des.*, 2006, **27**, p 529–534

4. M. Pietrzyk, FE Based Model of Structure Development in the Hot Rolling Process, *Steel Res.*, 1990, **61**, p 603–607
5. T. Reti and I. Felde, A Non-linear Extension of the Additivity Rule, *Comput. Mater. Sci.*, 1999, **15**, p 466–482
6. J.W. Christian, *The Theory of Transformations in Metals and Alloys*, 2ndPergamon Press, Oxford, 1975, p 545–546
7. W.A. Johnson and R.F. Mehl, Reaction Kinetics in Processes of Nucleation and Growth, *Trans. Am. Inst. Mining Metall. Eng.*, 1939, **135**, p 416–442
8. L.A. Dobrza′nski and J. Trzaska, Application of Neural Networks to Forecasting the CCT Diagrams, *J. Mater. Process. Technol.*, 2004, **157-158**, p 107–113
9. S. Malinov, W. Sha, and Z. Guo, Application of Artificial Neural Network for Prediction of Time-Temperature-Transformation Diagrams in Titanium Alloys, *Mater. Sci. Eng. A*, 2000, **283**, p 1–10
10. Z. Sterjovski, D. Nolan, K.R. Carpenter, D.P. Dunne, and J. Norrish, Artificial Neural Networks for Modelling the Mechanical Properties of Steels in Various Applications, *J. Mater. Process. Technol.*, 2005, **30**, p 536–544
11. S. Kobayashi and S.I. Oh, *Metal Forming and the Finite Element Method*, Oxford University Press, Oxford, 1989
12. J.G. Lenard, M. Pietrzyk, and L. Cser, *Mathematical and Physical Simulation of the Properties of Hot Rolled Products*, Elsevier, Oxford, 1999
13. M.T. Hagan, H.B. Demuth, and M. Beale, *Neural Network Design*, PWS Publishing Company, Boston, 2002
14. T. Sheppard, M.A. Zaidi, P.A. Hollinshead, and N. Raghunathan, Structural evolution during the rolling of Aluminium alloys, in *Microstructural Control in Aluminium Alloys: Deformation, Recovery and Recrystallization*, E.H. Chia, and H.J. McQueen, Eds., New York, 27 February 1985, The Metallurgical Society Inc., 1986, p 19–43
15. B.K. Chen, P.F. Thomson, and S.K. Choi, Computer Modeling of Microstructure During Hot Flat Rolling of Aluminum, *Mater. Sci. Technol.*, 1992, **8**, p 72–77
16. H. Ahmed, M.A. Wells, D.M. Maijer, B.J. Howes, and M.R. Van Der Winden, Modelling of Microstructure Evolution During Hot Rolling of AA5083 Using an Internal State Variable Approach Integrated into an FE Model, *Mater. Sci. Eng.*, 2005, **A390**, p 278–290
17. C.M. Sellars, Modeling Microstructural Development During Hot Rolling, *Mater. Sci. Technol.*, 1990, **6**, p 1072–1081
18. J.S. Vetrano, C.A. Lavender, C.H. Hamilton, M.T. Smith, and S.M. Bruemmer, Superplastic Behavior in a Commercial 5083 Aluminum Alloy, *Scripta Metall. Mater.*, 1994, **30**, p 565–570